A Self-Checking Predictor-Corrector Algorithm for Efficient Evaluation of Reflector Antenna Radiation Integrals

Fernando J. S. Moreira, *Student Member, IEEE,* and Aluizio Prata, Jr., *Member, IEEE*

***Abstract*— An efficient algorithm for numerically evaluating diffraction integrals is presented. The algorithm employs a predictor-corrector scheme combined with Ludwig's integration procedure. The predictor-corrector eliminates the amplitude and phase ambiguities present in the real+imaginary algebra used in machine calculations and provides accuracy self-checking capabilities. The end result is a reliable and efficient integration method that does not require independent integrand phase information, can handle arbitrarily shaped integration domains, and is capable of monitoring its own accuracy as the integration proceeds. The performance of the algorithm is investigated by computing, using the Physical Optics technique, the electromagnetic field scattered by representative reflector antenna geometries. These tests demonstrate that the proposed algorithm is particularly efficient in the analysis of multi-reflector systems.**

I. Introduction

In the determination of the diffraction of electromagnetic and acoustic waves by material objects and apertures one frequently faces the task of numerically evaluating integrals of the form

$$I = \int\int_S A(u,v)e^{jkB(u,v)}du\ dv, \tag{1}$$

where S is a surface integration domain, u and v are the corresponding integration variables, Ae^{jkB} is a function dependent of the field impinging on the aperture or object, and $k = 2\pi/\lambda$ (where λ is the radiation wavelength). In the case of electromagnetic fields, the above integral represents any one of the associated vector components. Herein we suppose that $A(u,v)$ and $kB(u,v)$ are both real functions, representing the complex amplitude and phase of the integrand, respectively. In most situations the functions $A(u,v)$ and $B(u,v)$ vary relatively slowly with the u and v coordinates. However, the presence of the constant k in the phase of the integrand causes its associated real and imaginary parts to vary (oscillate) rapidly. Due to this characteristic, the accurate evaluation of the above integral using standard numerical techniques (e.g., Simpson's rule, Newton-Cotes formulas, Gaussian quadratures, etc.), which basically interpolate the integrand by piecewise polynomials, requires considerable amount of integrand sample points. To overcome this difficulty, Ludwig's algorithm has been proposed [1]. In it the integration domain is divided into a mosaic of integration cells. Over each cell two first degree polynomials (i.e., planar functions) are used to independently approximate the amplitude and phase of the integrand. This interpolated integrand is then integrated in closed form yielding the desired final result. The advantage of this method is that the oscillatory behavior of the integrand's real and imaginary parts is avoided, yielding accurate results with smaller number of integrand evaluations.

Although numerically efficient, the application of Ludwig's algorithm to the above integral requires considerable special care. The reason for this resides on the fact that machine computations involving complex numbers are performed using their corresponding real and imaginary parts. Unambiguous amplitude and phase information is hence not directly available. To eliminate this difficulty, geometrical-optics concepts can be invoked. However, this procedure is strongly dependent of the geometry of the system under consideration and is troublesome to apply in many instances. The final consequence is a loss of generality on Ludwig's integration algorithm.

This work presents an algorithm capable of overcoming the difficulties mentioned in the previous paragraph—the Predictor-Corrector Integration Algorithm (PCIA). A predictor-corrector scheme is developed and incorporated in the Ludwig's integration algorithm, allowing it to be used without absolute integrand phase information. The predictor-corrector determines the unambiguous amplitude and phase values of the integrand, with the added benefit of providing an estimative of the integration procedure accuracy, producing a general and efficient integration method that maintains all the advantages of Ludwig's algorithm while eliminating some of its shortcomings.

II. The Integrator

It is demonstrated in Ref. [2] that, for electromagnetic scattering problems, Ludwig's algorithm performs better when applied in cartesian than in polar coordinates. The basic reason for this is the fact that $A(u,v)$ and $B(u,v)$ behave more smoothly when u and v are cartesian coordinates. In order to take advantage of this characteristic on integrations over surfaces enclosed by arbitrary rims, while representing the rim accurately, it is computationally more efficient to divide the integration domain into triangular cells and to use the variation of Ludwig's algorithm presented in Refs. [3] and [4]. Then, to

Manuscript received June 19, 1993; revised September 20, 1993.

The authors are with the University of Southern California, Los Angeles, CA 90089-0271.

IEEE Log Number 9215657.

perform the integration indicated by (1) using the PCIA, the domain S must first be divided into a mosaic of triangular cells and the amplitude and phase of the integrand must be known at each triangle vertex (nodes of the integration grid). These tasks are addressed later in this work. For now it is assumed that both the triangular cells and the unambiguous amplitude and phase values of the integrand at the nodes are available. One then can rewrite (1) as

$$I = \sum_{c=1}^{N_c} I_c, \tag{2}$$

where N_c is the total number of integration cells and I_c is the c-th cell integration result. This section concentrates on the evaluation of the I_c of each triangular cell.

To evaluate I_c one first assumes that independent interpolation of the amplitude and phase of the integrand by planar functions of the form

$$A_c(u,v) = A_u u + A_v v + A_o \text{ and } B_c(u,v) = B_u u + B_v v + B_o, \tag{3}$$

respectively, is possible. In the above equations, u and v are cartesian coordinates and the subscript c stresses the fact that the interpolation coefficients are cell dependent.

It is pointed out in Ref. [4] that a convenient coordinate system to analytically evaluate a surface integral over a triangular cell are the simplex (or natural) coordinates p and q. In this coordinate system the integral I_c can be rewritten as [4]

$$I_c \int_0^1 \int_0^{1-p} C_c(p,q) e^{jD_c(p,q)} dq\, dp, \tag{4}$$

where

$$C_c(p,q) = C_p p + C_q q + C_o \text{ and } D_c(p,q) = D_p p + D_q q + D_o. \tag{5}$$

In the above equations the C and D coefficients are given by

$$C_p = A_{c,1} - A_{c,3} \qquad C_q = A_{c,2} - A_{c,3} \qquad C_o = A_{c,3} \tag{6}$$

$$D_p = k(B_{c,1} - B_{c,3}) \quad D_q = k(B_{c,2} - B_{c,3}) \quad D_o = kB_{c,3} \tag{7}$$

where $A_{c,i}$ and $kB_{c,i}$ are the amplitude and phase values of the integrand at the i-th vertex of the triangular cell, respectively (see Fig. 1). The I_c integral can then be evaluated analytically yielding

$$I_c = 2S_c e^{jD_o} \left\{ e^{jD_p} \left[\frac{C_p + C_o}{D_p(D_q - D_p)} + F_1 - F_2 \right] - e^{jD_q} \left[\frac{C_q + C_o}{D_q(D_q - D_p)} - F_2 \right] - \frac{C_o}{D_p D_q} - F_1 \right\}, \tag{8}$$

where S_c is the area of the triangular cell (in the u and v coordinates) and

$$F_1 = \frac{j}{D_p D_q} \left(\frac{C_p}{D_p} + \frac{C_q}{D_q} \right),$$
$$F_2 = \frac{j}{D_q(D_q - D_p)} \left(\frac{C_p - C_q}{D_q - D_p} - \frac{C_q}{D_q} \right). \tag{9}$$

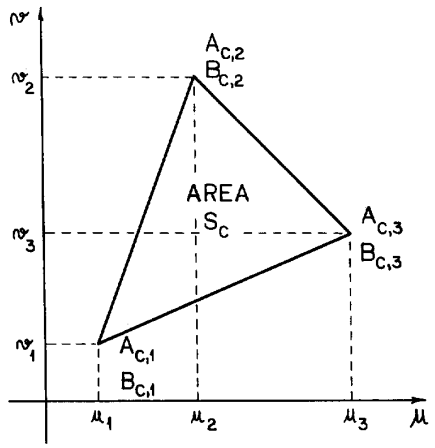

Fig. 1. Integration cell geometry.

The above I_c expression has removable singularities that become numerically troublesome whenever $|D_p|$, $|D_q|$, and $|D_q - D_p|$ are small. To handle these special cases, simple and efficient expressions can be obtained by expanding the term e^{jD_c} of (4) in a Taylor series about the appropriate small parameter and analytically integrating the resultant series term by term:

- If $|D_p| < L_t$ and $|D_q| \geq L_t$ (no restrictions on $|D_q - D_p|$)

$$I_c = 2S_c \frac{e^{jD_o}}{jD_q} \sum_{n=0}^{\infty} \frac{(jD_p)^n}{n!} \left\{ \frac{1}{n+1} \left(-C_o + \frac{C_q}{jD_q} \right) - \frac{C_p}{n+2} + e^{jD_q} \left[\left(C_q + C_o - \frac{C_q}{jD_q} \right) G(n, -D_q) + (C_p - C_q) G(n+1, -D_q) \right] \right\}, \tag{10}$$

- If $|D_p| < L_t$ and $|D_q| < L_t$ (no restrictions on $|D_q - D_p|$)

$$I_c = 2S_c e^{jD_o} \sum_{n=0}^{\infty} \sum_{m=0}^{\infty} \frac{(jD_p)^n (jD_q)^m}{(n+m+2)!} \times \left[C_o + \frac{C_p(n+1) + C_q(m+1)}{n+m+3} \right], \tag{11}$$

- If $|D_p| \geq L_t$ and $|D_q| < L_t$ (no restrictions on $|D_q - D_p|$)

$$I_c = 2S_c e^{jD_o} e^{jD_p} \sum_{n=0}^{\infty} \frac{(jD_q)^n}{n!} \left[\frac{C_p + C_o}{n+1} G(n+1, -D_p) + \left(\frac{C_q}{n+2} - \frac{C_p}{n+1} \right) G(n+2, -D_p) \right], \tag{12}$$

- If $|D_p| \geq L_t$, $|D_q| \geq L_t$, and $|D_q - D_p| < L_t$

$$I_c = 2S_c \frac{e^{jD_o}}{jD_q} \sum_{n=0}^{\infty} \frac{[j(D_p - D_q)]^n}{n!} \times \left\{ \left(-C_o + \frac{C_q}{jD_q} \right) G(n, D_q) - C_p G(n+1, D_q) + e^{jD_q} \left[\frac{1}{n+1} \left(C_q + C_o - \frac{C_q}{jD_q} \right) + \frac{C_p - C_q}{n+2} \right] \right\}, \tag{13}$$

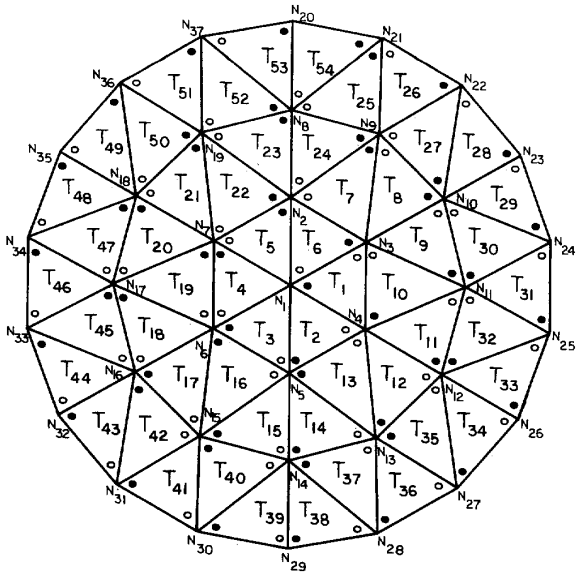

Fig. 2. Division of a circular integration domain in triangular cells.

where

$$G(n,w) = \int_0^1 s^n e^{jws} ds. \tag{14}$$

The function $G(n,w)$ can be evaluated recursively using the relation

$$G(n,w) = \frac{e^{jw} - nG(n-1,w)}{jw}, \text{for } n \geq 1, \tag{15}$$

together with the startup value $G(0,w) = (e^{jw}-1)/(jw)$.

Equations 10–15 are numerically efficient since, in all tested applications, very accurate results have been obtained by setting $L_t = 0.05$ and using only terms with $n,m \leq 2$ in the series. Furthermore, they are only needed on the relatively small number of occasions where (8) has numerical difficulties. To save computation time, it is crucial to use (7) to break down the complex exponentials of (8). This allows the exponentials to be calculated only once for each grid node.

The above procedure can be applied to any arbitrary domain S, as long as it is first divided into a mosaic of triangular cells. Of particular relevance to reflector antenna applications is the case of a circular integration domain—a very common projected aperture shape. The division of this domain can be performed by creating six equiangular radial sectors and N_A concentric rings of identical width (see Fig. 2), and dividing each ring as shown in the figure. The n_A-th ring contains $6(2n_A - 1)$ triangular cells. This process yields triangles with similar dimensions, allows control of the average area of the triangles by a single parameter (N_A), and permits a convenient way to enumerate the cells, vertices, and nodes. Proper enumeration schemes are essential for the predictor-corrector operation—convenient ones are depicted in Fig. 2 and discussed in more detail at the end of next section.

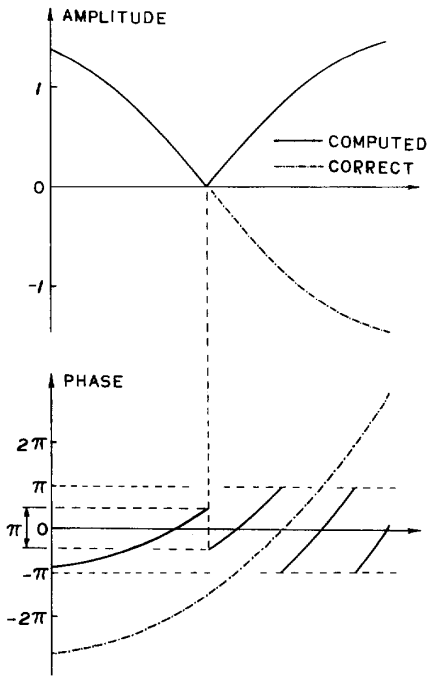

Fig. 3. Amplitude and phase ambiguities present in machine computations.

III. The Predictor-Corrector

The predictor-corrector algorithm operates by estimating (predicting) the phase values of the integrand at the vertices of the triangular cells and using these estimated values to eliminate (correct) any $n2\pi$ radians ($n = 0, \pm 1, \pm 2, \ldots$) and sign ambiguities present in the phase and amplitude, respectively. These ambiguities are inherent to the real+imaginary complex algebra that must be used to perform computations—phase values are determined within a 2π radians range and amplitude values are always positive. This behavior leads to discontinuities in the phase function $kB_c(u,v)$ and in the derivatives of the amplitude function $A_c(u,v)$, as exemplified by Fig. 3, and precludes the correct interpolation of the integrand of (1) as required by Ludwig's algorithm.

The predictor step basically consists of indirectly using (3) to extrapolate (predict) the phase value of the integrand from a cell into its adjacent one. To demonstrate how this is done, we start by referring to Fig. 4 and by assuming that the correct phase values $kB_{c,1}$, $kB_{c,2}$, and $kB_{c,3}$ are available at the three vertices of an arbitrary cell T_c. The determination of the three unambiguous phase values for the vertices of the first cell T_1 is addressed near the end of this section.

Let us consider initially only the problem of determining the phase at the vertex $V_{c+1,3}$, belonging to the cell T_{c+1}. To determine this phase one first constructs a plane passing through the tip of the vectors $\hat{b}kB_{c,1}$, $\hat{b}kB_{c,2}$, and $\hat{b}kB_{c,3}$, in the u,v,kB tri-dimensional space, as shown in Fig. 4. This plane can then be used to perform a linear extrapolation and hence predict the phase value $kB'_{c+1,3}$ at the vertex $V_{c+1,3}$. A convenient expression for $kB'_{c+1,3}$ can be obtained recalling

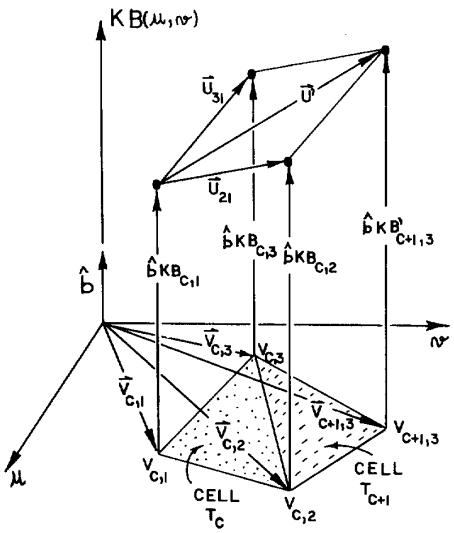

Fig. 4. Predictor-corrector linear extrapolation scheme.

that

$$\vec{U}' \cdot \left(\vec{U}_{21} \times \vec{U}_{31}\right) = 0. \tag{16}$$

Substituting in this expression

$$\vec{U}' = \left(\vec{V}_{c+1,3} + \hat{b}kB'_{c+1,3}\right) - \left(\vec{V}_{c,1} + \hat{b}kB_{c,1}\right), \tag{17}$$

one then obtains

$$kB'_{c+1,3} = \frac{\left(\vec{V}_{c,1} + \hat{b}kB_{c,1} - \vec{V}_{c+1,3}\right) \cdot \left(\vec{U}_{21} \times \vec{U}_{31}\right)}{\hat{b} \cdot \left(\vec{U}_{21} \times \vec{U}_{31}\right)}, \tag{18}$$

where $\vec{U}_{21}$ and $\vec{U}_{31}$ are given by (with $i = 2$ or 3, respectively)

$$\vec{U}_{i1} = \left(\vec{V}_{c,i} + \hat{b}kB_{c,i}\right) - \left(\vec{V}_{c,1} + \hat{b}kB_{c,1}\right). \tag{19}$$

Having predicted the phase $kB'_{c+1,3}$ at the vertex $V_{c+1,3}$, one then proceeds to use this value to remove the ambiguities present in the computed integrand value—the corrector step. We know that the correct, the predicted, and the computed (i.e., value with ambiguity) integrand values, at the vertex $V_{c+1,3}$, are

$$G|_{\text{correct}} = A_{c+1,3}\angle kB_{c+1,3}, \tag{20}$$

$$G|_{\text{predicted}} = A'_{c+1,3}\angle kB'_{c+1,3}, \tag{21}$$

$$G|_{\text{computed}} = |A_{c+1,3}|\angle kB''_{c+1,3}, \tag{22}$$

respectively, where $-\pi < kB''_{c+1,3} \leq +\pi$. We also know that

$$A_{c+1,3} = \sigma|A_{c+1,3}|, \tag{23}$$

$$kB_{c+1,3} = kB''_{c+1,3} + 2n\pi + (\sigma - 1)\pi/2, \tag{24}$$

where n is an integer (positive, negative, or equal to zero) and σ is either $+1$ or -1, depending on $A_{c+1,3} \geq 0$ or $A_{c+1,3} < 0$, respectively. To solve this equation for n and σ, $kB_{c+1,3}$ is replaced by the predicted value $kB'_{c+1,3}$ in (24) (since $kB_{c+1,3}$ is unknown and $kB'_{c+1,3}$ is supposed to be a good approximation for it) and two values for n are determined:

$$n^{+}_{-} = \text{closest integer to } \left(\frac{kB'_{c+1,3} - kB''_{c+1,3} - (\sigma - 1)\pi/2}{2\pi}\right), \tag{25}$$

corresponding to σ equal to $+1$ and -1, respectively. Next, the two n,σ pairs are substituted back into (24), with $kB_{c+1,3}$ replaced once more by the predicted value $kB'_{c+1,3}$, to determine the error ϵ of the predicted phase value:

$$\epsilon = \left|kB'_{c+1,3} - [kB''_{c+1,3} + 2n\pi + (\sigma - 1)\pi/2]\right|. \tag{26}$$

The pair yielding the smallest ϵ is the correct one. Finally, once the n and σ values are known, the corrected (without ambiguity) amplitude and phase values of the integrand can be written as

$$G|_{\text{correct}} = \sigma|A_{c+1,3}|\angle\left[kB''_{c+1,3} + 2n\pi + (\sigma - 1)\pi/2\right]. \tag{27}$$

A closer look at the corrector step shows that it is based on the assumption that the predicted and corrected phase values are close to each other. Consequently, if the dimensions of the integration cells are excessive, the linear extrapolation used to predict the phase will be inaccurate and the algorithm will fail. However, if the interpolating function fails to accurately perform the required extrapolation, then it most probably will fail to interpolate the integrand over the cell, and the accuracy of the PCIA is lost anyhow. This fact constitutes the basis of the self-checking characteristic of the proposed algorithm. By monitoring the magnitude of the error ϵ one can determine if the planar functions $A_c(u, v)$ and $B_c(u, v)$ are sufficiently accurate interpolators. If not, the size of the integration cells must be reduced. The maximum tolerable error ϵ_M depends on both the integrand behavior and on the desired integral accuracy. By monitoring the integral convergence as the size of the cells is decreased, it is usually possible to obtain an estimative for the maximum tolerable ϵ_M value, applicable for each class of problems.

Note that if the value of the amplitude $|A_{c+1,3}|$ is sufficiently small, roundoff errors will produce a $G|_{\text{computed}}$ with an incorrect phase $kB''_{c+1,3}$. The use of this non-reliable phase value into the corrector step (25)–(27) will yield a wrong $G|_{\text{correct}}$. This error will then propagate to all subsequent nodes, destroying the algorithm accuracy. This problem can be circumvented by continuously monitoring the amplitude $|A_{c+1,3}|$ of the computed value and, whenever it becomes too small, the corrector step is not performed and the predicted phase value is used as the corrected one. This substitution is effective because, when the algorithm is working properly, the error ϵ is small.

As demonstrated above, once the correct amplitude and phase values are known at the vertices of any cell of the integration domain, the correct amplitude and phase values at the vertices of all remaining cells can be obtained using the predictor-corrector. The first requirement of the predictor-corrector is then to obtain the correct values of the integrand at the initial cell. However, since the predictor-corrector always requires three nodes to start marching, it can not be used to

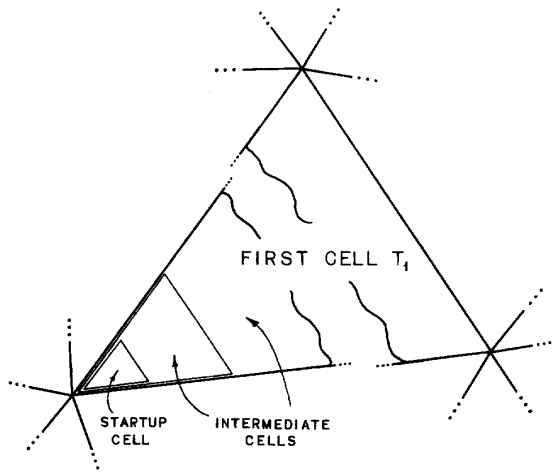

Fig. 5. Starting cells of the predictor-corrector procedure.

start itself. Due to this fact, it is essential to start the predictor-corrector scheme with a sufficiently small cell (the startup cell) to guarantee that the $A_c(u,v)$ amplitudes are not zero anywhere on its interior (so that they all can be arbitrarily assumed positive) and $kB_c(u,v)$ changes by less than π radians from any vertex to its adjacents (so that the phases can be determined without the predictor-corrector). Starting with this small startup cell, the integrand values can then be subsequently predicted and corrected while progressively enlarging the cell (intermediate cells), until any desired size is attained (see Fig. 5). Once the correct integrand values are determined over the first cell (T_1), the predictor-corrector algorithm starts marching accordingly to the procedure presented in the previous paragraphs, proceeding into the second cell T_2, third cell T_3, and so on. In practice some redundancy is also recommended. It can be achieved by setting two startup cells inside T_1 and checking to verify that they yield the same phase values at all three T_1 vertices. For all cases studied in this work, the dimensions of the startup cell sides are approximately 0.1λ.

The previous section shows how the division of a circular domain S into a mosaic of triangular cells can be efficiently performed. This division also yields a convenient scheme for ordering cells, vertices and nodes, as shown in Fig. 2. First of all, the startup cell is located inside cell T_1 at the node N_3, away from the center of the grid and the symmetry axes, regions where, in reflector antenna analysis, the amplitude $A_c(u,v)$ have more probability of being zero. Both the predictor-corrector and integrator go through the depicted cells sequentially: T_1, T_2, T_3, etc. Also shown in the figure are small open and solid circles, two inside each cell. The open and solid circles of cell T_c are its vertices $V_{c,1}$ and $V_{c,3}$, respectively. Also, the solid circle of cell T_{c+1} is the vertex $V_{c+1,3}$, in accordance to Fig. 4. A convenient ordering of the grid elements is also important to avoid unnecessary usage of the predictor-corrector scheme over the same node more than once.

The proper ordering of the triangular cells also yields an useful alternative self-checking procedure: the prediction and correction of the phase at selected nodes twice. To demonstrate this technique consider once again the circular integration domain (Fig. 2). Starting at the cell T_1, the predictor-corrector is used throughout the first ring arriving at the cell T_6. However, as cells T_1 and T_6 share the common node N_3, their phase values at this node must be identical. If this is indeed true, all is well and the predictor-corrector proceeds into the next adjacent cell T_7 in the second ring, marches all the way to cell T_{24}, checks the phase agreement once more at node N_9 (common to cells T_7 and T_{24}), and so on. If the phase checking does not agree at any point, an error has occurred, indicating that excessively large cells are being used. The algorithm must then be halted, the parameter N_A increased, and the whole procedure restarted from the beginning.

It is possible to encounter integrands that can not be handled efficiently by the PCIA. A typical situation is presented in the Appendix and is generally found in feed-array applications. However, in such cases the two self-checking schemes presented previously will detect the problem.

IV. Reflector-Antenna Scattering Results

To investigate the performance of the PCIA in practical applications the radiation patterns of an offset paraboloid, an axially symmetric hyperboloid, and an offset Gregorian system have been computed. They are shown in Figs. 6–8, together with the corresponding geometries. All test cases have circular projected exit apertures of diameter D and have been excited by a perfectly xz-plane linearly-polarized raised-cosine feed (according to Ludwig's third polarization definition [5]). This feed radiates a spherical wave with amplitude pattern described by $\cos^h \theta_F$, where θ_F is the angle measured from the feed boresight direction and h is a parameter that controls the pattern taper.

The Physical Optics (PO) technique has been employed to determine all scattered fields [6]. The u and v coordinates used in all associated integrals were the projected aperture-plane x and y coordinates, respectively. With exception of the subreflector of the dual-reflector geometry, all integration domains are circular and have been divided in cells according to Fig. 2. For the subreflector the integration domain is elliptical. However, it has also been divided in cells according to Fig. 2—using spherical coordinates originating at the system focus, with the center point of Fig. 2 coinciding with the subreflector angular center. This produces somewhat larger area differences among the triangular cells (in the u,v plane), but the differences are still tolerable and computer coding is simplified. In all test cases six intermediate triangular cells have been used to start the predictor-corrector scheme (including the startup one). This yields twelve extra nodes, in addition to the ones depicted in the grid of Fig. 2.

In all geometries the rotated spherical components of the far-zone electric field integrand $E_{\theta'}$ and $E_{\phi'}$ have been employed in the computations. They are given by

$$E_{\theta'} = E_\theta \cos(\phi - \phi_r) - E_\phi \sin(\phi - \phi_r), \quad (28)$$

$$E_{\phi'} = E_\theta \sin(\phi - \phi_r) + E_\phi \cos(\phi - \phi_r), \quad (29)$$

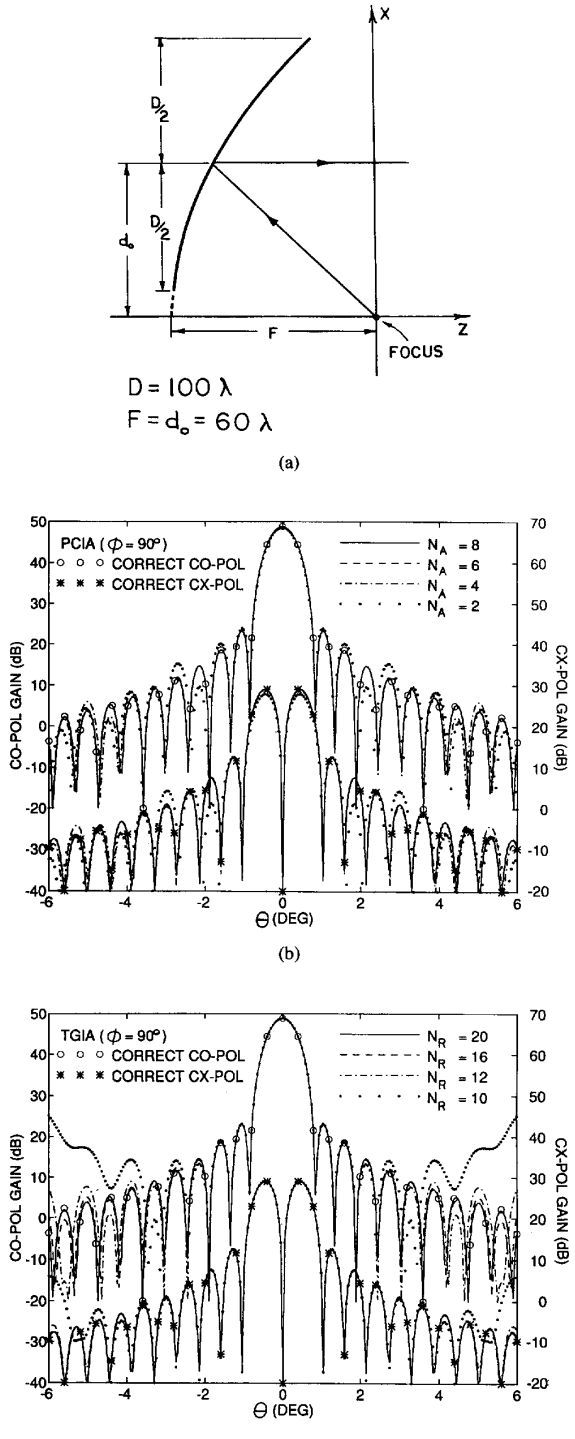

Fig. 6. Offset paraboloidal reflector antenna test case: a) Antenna geometry; b) PCIA pattern results; c) TGIA pattern results.

where $\phi_r = \pi/4$, and E_θ and E_ϕ are the components of the spherical coordinate system associated with the cartesian one shown in Figs. 6–8. Using these $\hat{\theta}'$- and $\hat{\phi}'$-components, instead of the customary $\hat{\theta}$ and $\hat{\phi}$ ones, one elliminates potential predictor-corrector problems associated with small amplitude values plagued by roundoff errors. Note that $\phi_r = \pi/4$ in the above equations because the feed is polarized in the xz-plane. For a general linearly-polarized excitation, ϕ_r should be set to the feed polarization direction plus $\pi/4$. The scattered near-field produced by the subreflector of the Gregorian configuration has been evaluated using the three cartesian components of the integrand.

The results obtained with the PCIA have been compared with the ones obtained using a nested integration scheme in polar coordinates, herein called TGIA (Trapezoidal Rule and Gauss-Legendre Quadrature for the azimuthal and radial integrations, respectively) [7]. The number of integration points along the rim has been set equal to the optimum value of four times the number of rings (N_R). For the inner rings, it has been reduced in proportion to the ring radius. All numerical results were obtained using a SUN Microsystems SPARCstation 10.

The first test case considered is the offset paraboloidal reflector shown in Fig. 6a. The antenna is illuminated by a focused feed with $h = 4.9$, aimed at the reflector point with coordinates $x = d_0$ and $y = 0$. The second test case corresponds to the Rusch subreflector [8] (see Fig. 7a), illuminated by a feed with $h = 0$, aimed at the hyperboloid vertex, and located at the outer focus. The third and last test case is the dual-reflector geometry of Fig. 8a. This antenna was designed using Ref. [9], to provide optimum cross-polarization and spillover performance. A feed with $h = 30.87$, placed at the system focus and aimed at the subreflector angular center, has been used for its excitation. Figs. 6–8 depict the corresponding far-zone radiation patterns, using the PCIA and the TGIA. 241, 161, and 241 equispaced points along the $\hat{\theta}$ direction ($\phi = 90°$) have been used to determine the radiation patterns for test cases 1, 2, and 3, respectively. To avoid cluttering the patterns of test case 1, the co- and cross-polarized plots are shown using different scales.

The basic characteristics of the PCIA and TGIA are summarized on Tables I and II, respectively. For the dual-reflector test case, in the columns containing two values separated by semicolon, the first and second numbers correspond to the main and subreflectors integrations, respectively (similar for the N_A and N_R values shown in the patterns). From the tables and radiation pattern results we can conclude that, for single-reflector systems, the PCIA and the TGIA provide comparable accuracy and numerical efficiency. However, the PCIA yields more stable results while requiring considerably less number of integration nodes. Because of this number-of-nodes reduction, the PCIA is capable of evaluating the radiation patterns of dual-reflector antennas with considerably less computational time. Table I also depicts the maximum phase difference ϵ_M between the predicted and the corrected values, among all grid nodes (ϵ_M is practically independent of the integrand vector component being considered). These values demonstrate the typical accuracy of the predictor step and can be used to implement the PCIA self-checking procedure.

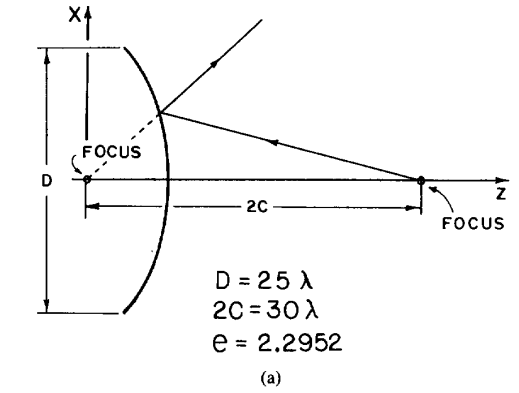

(a)

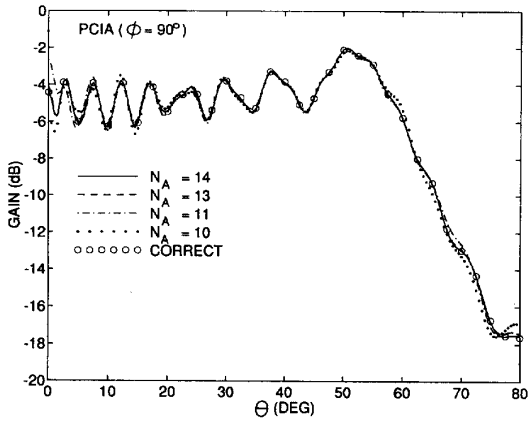

(b)

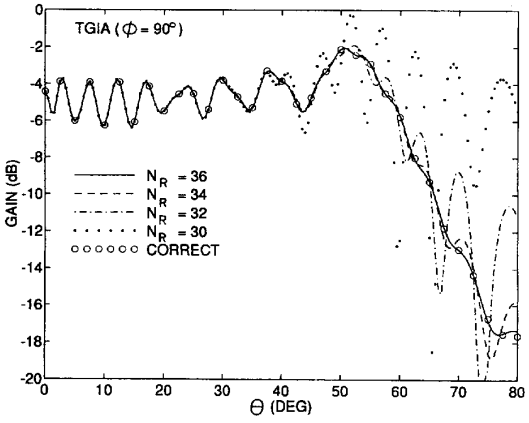

(c)

Fig. 7. Axially symmetric hyperboloidal subreflector antenna test case: a) Antenna geometry; b) PCIA pattern results; c) TGIA pattern results.

V. Conclusion

An integration algorithm for numerically evaluating the double integrals encountered in scattering computations has been developed and tested. The algorithm is based on a triangular-cell implementation of Ludwig's algorithm, augmented by a

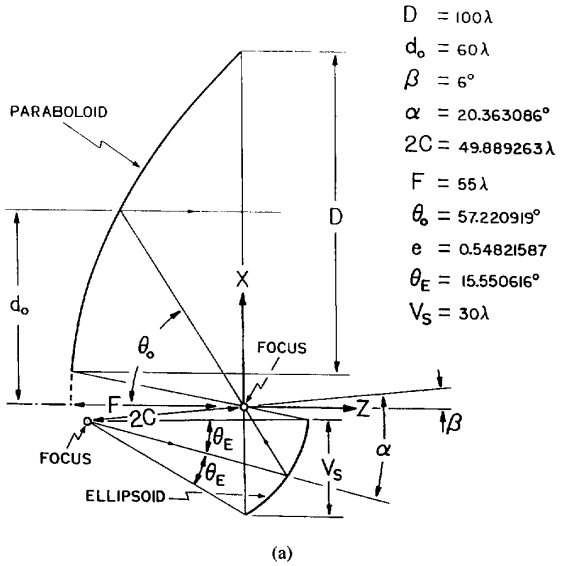

(a)

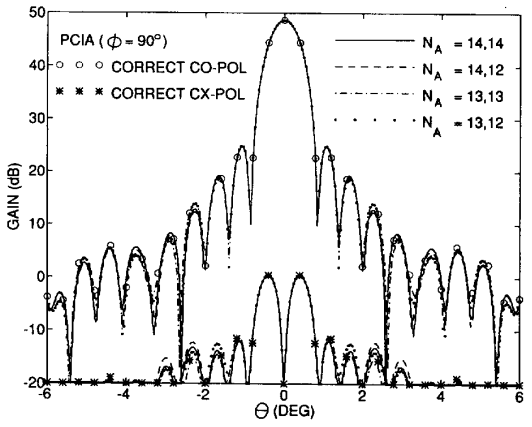

(b)

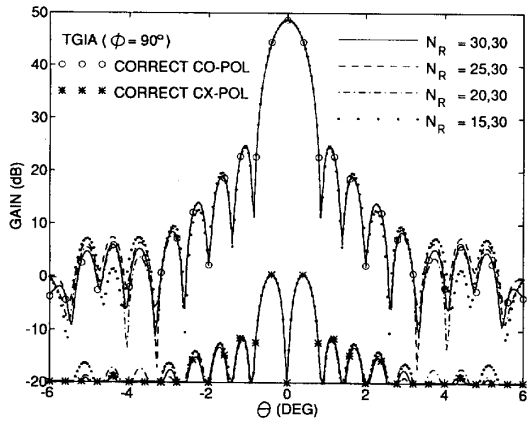

(c)

Fig. 8. Offset dual-reflector Gregorian antenna test case: a) Antenna geometry; b) PCIA pattern results; c) TGIA pattern results.

TABLE I
PCIA NUMERICAL RESULTS

Case	N_A	Nodes	CPU (sec)	ϵ_M
1	8	217	6.7	0.7°
	6	127	4.0	1.2°
	4	61	2.0	2.5°
	2	19	0.8	9.1°
2	14	631	10.9	32°
	13	547	9.7	37°
	11	397	6.9	51°
	10	331	5.8	60°
3	14; 14	631; 631	89	13°; 32°
	14; 12	631; 469	71	14°; 45°
	13; 13	547; 547	69	16°; 38°
	13; 12	547; 469	61	16°; 44°

TABLE II
TGIA NUMERICAL RESULTS

Case	N_R	Nodes	CPU (sec)
1	20	792	4.0
	16	506	2.7
	12	284	1.6
	10	197	1.2
2	36	2,578	8.7
	34	2,299	7.8
	32	2,036	6.9
	30	1,789	6.1
3	30; 30	1,789; 1,789	142
	25; 30	1,240; 1,789	97
	20; 30	792; 1,789	62
	15; 30	445; 1,789	35

predictor-corrector scheme. This combination constitutes the Predictor-Corrector Integration Algorithm (PCIA). The use of triangular cells renders the algorithm capable of handling arbitrarily shaped integration domains. The predictor-corrector scheme determines the unambiguous values of the integrand amplitude and phase at each integration-grid node, eliminating the need of independent phase information. Also, the predictor-corrector evaluates the accuracy of the PCIA as the integration is performed, providing a self-checking capability. Accurate expressions required to overcome the removable singularities present in Ludwig's triangular integrator have been presented.

The performance of the PCIA has been evaluated for a few representative reflector antenna geometries. When compared to a nested integration procedure using Trapezoidal Rule combined with Gauss-Legendre Quadrature, the results demonstrate that the PCIA drastically reduces the number of integrand sample points required to evaluate scattering integrals, in addition of providing more stable results. This makes the algorithm very efficient for multi-reflector antennas computations. However, since the PCIA is inherently more complex than the nested scheme, its computational burden is larger. Due to this fact, for the single reflector antenna geometries tested, the numerical efficiency of the PCIA is only slightly better than the one obtained with the nested scheme. Also, due to inherent characteristics of the predictor-corrector, the PCIA is not able to handle integrands with an ill-behaved phase, such as the ones encountered when handling reflectors illuminated by feed arrays. As a final comment it must be pointed out that, although only a triangular-cell version of the PCIA has been treated in this work, the predictor-corrector principle can successfully be incorporated into other integration algorithms (e.g., [10] and [11]).

VI. APPENDIX

Consider two well behaved, but otherwise arbitrary, complex functions represented by

$$G_1 = \Gamma_1 e^{j\Psi_1} \text{ and } G_2 = \Gamma_2 e^{j\Psi_2} = \gamma\Gamma_1 e^{j(\Psi_1+\psi)}, \quad (30)$$

where Γ_1, Ψ_1, γ, and ψ are real functions of the integration variables u and v, and let us investigate the behavior of their sum

$$\Lambda = \Gamma_1 e^{j\Psi_1}\left(1+\gamma e^{j\psi}\right). \quad (31)$$

This may represent, for example, the PO integrand of a reflector antenna illuminated by two feed elements. Rewriting the above equation in polar form one gets

$$\Lambda = \Gamma_1\sqrt{1+2\gamma\cos\psi+\gamma^2}\angle \cdot\left[\Psi_1 + \arctan\left(\frac{\gamma\sin\psi}{1+\gamma\cos\psi}\right)\right], \quad (32)$$

and taking the partial derivatives of $\angle\Lambda$ with respect to u and v yields

$$\frac{\partial\angle\Lambda}{\partial u,v} = \frac{\partial\Psi_1}{\partial u,v} + \frac{1}{1+2\gamma\cos\psi+\gamma^2} \times\left[\frac{\partial\gamma}{\partial u,v} + (1+\gamma^2)\frac{\partial\psi}{\partial u,v}\right], \quad (33)$$

which indicates a very fast phase variation whenever $\gamma \approx +1$ or -1 for $\psi \approx \pi$ or 0, respectively (i.e., when $G_1 \approx -G_2$). This demonstrates that, even if the partial derivatives of Ψ_1, Γ_1, γ, and ψ are well behaved, the partial derivatives of the phase of the sum $G_1 + G_2$ can be ill behaved, creating difficulties for the PCIA. The above result is readily extended to summations with more terms (e.g. integrands generated by feed-array excitation).

ACKNOWLEDGMENT

The authors are thankful to the reviewers for having brought to their attention the high numerical efficiency of the nested Trapezoidal Rule plus Gauss-Legendre Quadrature integration scheme. This fact has been incorporated in this work, and yielded a more precise accessment of the numerical efficiency of the PCIA.

REFERENCES

[1] A. C. Ludwig, "Computation of Radiation Patterns Involving Numerical Double Integration," *IEEE Trans. Antennas and Propagat.*, **AP-16**, No. 6, pp. 767–769, Nov. 1968.
[2] J. R. Parkinson and M. J. Mehler, "Convergence of Physical Optics Integrals by Ludwig's Technique," *Elec. Lett.*, **22**, No. 22, pp. 1161–1162, Oct. 1986.
[3] R. J. Pogorzelski, "The Ludwig Integration Algorithm for Triangular Subregions," *Proc. of the IEEE*, **73**, No. 4, pp. 837–838, April 1985.
[4] M. L. X. dos Santos and N. R. Rabelo, "On the Ludwig Integration Algorithm for Triangular Subregions," *Proc. of the IEEE*, **74**, No. 10, pp. 1455–1456, Oct. 1986.

[5] A. C. Ludwig, "The Definition of Cross Polarization," *IEEE Trans. Antennas and Propagat.*, **AP-21**, No. 1, pp. 116–119, Jan. 1973.
[6] W. V. T. Rusch and P. D. Potter: *Analysis of Reflector Antennas*, Academic Press, New York, 1970).
[7] W. L. Stutzman, S. W. Gilmore and S. H. Stewart, "Numerical Evaluation of Radiation Integrals for Reflector Antenna Analysis Including a New Measure of Accuracy," *IEEE Trans. Antennas and Propagat.*, **36**, No. 7, pp. 1018–1023, July 1988.
[8] W. V. T. Rusch, "Reflector Antennas," in *Numerical and Asymptotic Techniques in Electromagnetics*, R. Mittra, Ed., Springer-Verlag, New York, 1975, pp. 242–243.
[9] W. V. T. Rusch, A. Prata, Jr., Y. Rahmat-Samii and R. A. Shore, "Derivation and Application of the Equivalent Paraboloid for Classical Offset Cassegrain and Gregorian Antennas," *IEEE Trans. Antennas and Propagat.*, **38**, No. 8, pp. 1141–1149, August 1990.
[10] G. D. Crabtree, "A Numerical Quadrature Technique for Physical Optics Scattering Analysis," *IEEE Trans. Magnetics*, **27**, No. 5, pp. 4291–4294, Sep. 1991.
[11] F. J. S. Moreira and A. Prata, Jr., "A Predictor-Corrector Algorithm for the Numerical Evaluation of Reflector Antenna Radiation Integrals," *1993 IEEE AP-S Int. Symp. Digest*, Ann Arbor, Michigan, pp. 250–253, June 28–July 2, 1993.

Fernando J. S. Moreira (S'89) was born in Rio de Janeiro, Brazil, on July 18, 1967. He received the B.S. and M.S. degrees in Electrical Engineering from the Pontificia Universidade Catolica (Rio de Janeiro) in 1989 and 1992, respectively. He is currently at the University of Southern California working towards the Ph.D. degree in electrical engineering under a scholarship from the Brazilian agency CNPq. His main interests are applied electromagnetics and antennas.

Aluizio Prata, Jr. (S'84–M'90), was born in Uberaba, Brazil, on March 18, 1954. He received the B.S.E. degree in 1976 from the University of Brasilia, Brasilia, Brazil, the M.S. degree in 1979 from the Pontifical Catholic University of Rio de Janeiro, Rio de Janeiro, Brazil, and the Ph.D. degree in 1990 from the University of Southern California, all in electrical engineering. He also holds an M.S.E.E. degree from the California Institute of Technology, 1984.

From 1979 to 1983, he was with the Telebras Research and Development Center, Brazil, working on the design and construction of satellite earth station antennas. While at the California Institute of Technology he designed and implemented one of the first operational neural computers. Currently, he is an Assistant Professor at the University of Southern California, working with applied electromagnetics. He has been a consultant for several aerospace companies, and has authored or co-authored over 30 articles, patents, and symposium papers. He is a member of Sigma Xi and Eta Kappa Nu.